Translational Oncology 15 (2022) 101257

Contents lists available at ScienceDirect

Translational Oncology

journal homepage: www.elsevier.com/locate/tranon

Original Research

A monoclonal antibody against annexin A2 targets stem and progenitor cell fractions in tumors

Rajkumar S. Kalra [a,b,c,1], Gaurav S. Soman [a,1], Pradeep B. Parab [a], Avinash M. Mali [a], Sagar S. Varankar [a,b,d], Rutika R. Naik [a,b], Swapnil C. Kamble [a,b,e], Jaspreet K. Dhanjal [f], Sharmila A. Bapat [a,b,*]

[a] National Centre for Cell Science, NCCS Complex, Savitribai Phule Pune University Campus, Pune 411007, India
[b] Savitribai Phule Pune University, Ganeshkhind, Pune 411007, India
[c] Immune Signal Unit, Okinawa Institute of Science and Technology Graduate University, 1919-1 Tancha, Onna-son, Okinawa, 904-0495, Japan
[d] Wellcome-MRC Cambridge Stem Cell Institute, Puddicombe Way, Cambridge, CB2 0AW
[e] Department of Technology, Savitribai Phule Pune University, Ganeshkhind, Pune 411007, India
[f] Department of Computational Biology, Indraprastha Institute of Information Technology Delhi, Okhla Industrial Estate, Phase III, New Delhi 110020, India

ARTICLE INFO

Keywords:
Monoclonal antibody
Annexin A2
Cancer stem cells
Progenitors
Epigenetic potentiation
Active cooperative cell migration

ABSTRACT

The involvement of cancer stem cells (CSCs) in driving tumor dormancy and drug resistance is well established. Most therapeutic regimens however are ineffective in targeting these regenerative populations. We report the development and evaluation of a monoclonal antibody, mAb150, which targets the metastasis associated antigen, Annexin A2 (AnxA2) through recognition of a N-terminal epitope. Treatment with mAb150 potentiated re-entry of CSCs into the cell cycle that perturbed tumor dormancy and facilitated targeting of CSCs as was validated by in vitro and in vivo assays. Epigenetic potentiation further improved mAb150 efficacy in achieving total tumor regression by targeting regenerative populations to achieve tumor regression, specifically in high-grade serous ovarian adenocarcinoma.

Highlights-

Monoclonal antibody; ANXA2; novel epitope; cancer stem cells; progenitors

Introduction

Disease relapse in cancer is often mediated by a small quiescent population of cancer stem cells (CSCs), which escape chemotherapy and adoptively propagate new tumors [1]. The notorious characteristics of CSCs viz. self-renewal, multi-lineage differentiation, tumor initiation, invasion/migration, and drug resistance are presently realised as roadblocks in contemporary therapeutics [2–4]. Most promising drugs at the pre-clinical levels often eliminate rapidly proliferating cells within tumors. This is an incomplete evaluation of drug cytotoxicity since it fails to account for slow-cycling or quiescent populations that contribute to disease relapse and compromise the efficacy of therapeutic regimens [2–4]. This necessitates the development of specific drugs that could target CSCs and other dormant/ slow-cycling populations within tumors. Monoclonal antibody (mAb)-based immunotherapy promises specific targeting of tumor cells with minimal side effects and an added benefit of resurrecting host immune responses [5,6]. Several mAbs approved by Food and Drug Administration (FDA), USA, are reportedly successful in diverse cancers in the clinic including rituximab, trastuzumab, cetuximab, bevacizumab, and nivolumab; additional mAbs are either under FDA review or in phase 3 trials [7]. The clinical success of immune checkpoints inhibitors (ICI) viz. ipilimumab, tremelimumab, nivolumab, pidilizumab, atezolizumab and durvalumab further emphasizes the utility of mAbs against immune checkpoints such as CTLA-4, PD-1, and PDL-1 in solid tumors [6]. These successes, however, do not address the elimination of CSCs and other dormant/slow-cycling tumor cell populations which could reduce the risk of relapse.

In the present report, we developed and characterized a monoclonal antibody viz. mAb150 that recognizes a 37 kDa antigen, consequently

* Corresponding author at: National Centre for Cell Science, NCCS Complex, Pune 411007, India.
E-mail address: sabapat@nccs.res.in (S.A. Bapat).
[1] Equal contribution authors

https://doi.org/10.1016/j.tranon.2021.101257
Received 23 August 2021; Received in revised form 19 October 2021; Accepted 20 October 2021
Available online 27 October 2021

identified as Annexin A2 (AnxA2/Annexin II). AnxA2 is a member of Annexin family of calcium-dependent phospholipid-binding proteins and is associated with several metastatic cancers [8]. The epitope recognized by mAb150 was identified at the N-terminal of AnxA2, which is essential for membrane localization and interactions with binding partners such as S100A10 [9]. Profiling AnxA2 expression across heterogeneous tumor cell populations revealed a high specificity of mAb150 for AnxA2-expressing CSC and progenitor populations in xenografts, hence treatment with mAb150 could significantly reduce tumor burden by targeting these populations. Analysis of AnxA2 expression networks and protein interactions further elucidated its contributions to cell migration and tumor metastasis. Treatment with mAb150 was also found to delay ascites formation and prolong survival in ovarian cancer xenograft models, which affirms its efficacy.

Methods

Drugs, cells, PKH labeling, tumor xenograft and treatment regimens

All drugs and basic cell culture/biochemistry/proteomics reagents were procured from Sigma-Aldrich (St. Louis, MO, USA) unless otherwise specified. A4, OVCAR3 and other cell lines were procured and cultured as described earlier [10]. PKH67 labeling of cells and generation of xenografts (labeled / unlabeled) has been described earlier [11, 12]; subcutaneous injections of 5×10^6 for OVCAR3 or 2.5×10^6 cells for rest of the cell lines in 6–8-week-old female NOD/SCID mice were administered. MCF7 xenografts were developed with prior estradiol treatment as per established protocol [13]. Mice were bred and maintained at the NCCS Experimental Animal Facility; all procedures were carried out in accordance with the Institutional Ethical Animal Committee's clearances, laws, and policies. mAb150 treatment was administered once tumors were palpable, as 3 injections per week (3D,150 μg protein/site) for 2 weeks followed by a week of recovery or 3 injections per week X 2 (6D). 5Aza-dC and HMTase inhibitor were administered 15 days after initiation of A4 subcutaneous xenografts at tumor site in NOD/SCID mice at a final drug concentration of 5 mg/kg of body weight. On harvesting, tumor volumes were calculated as: Tumor Volume = Length x $(\text{Width}^2)/2$ cm^3 [14]. The PDX model was developed from tumor ascites obtained from a 65-year-old high grade serous ovarian cancer patient who presented with recurrent disease following two years of Paclitaxel-Carboplatin-NACT and liposomal doxycycline treatment. Ascites derived cells were washed 2–3 times with plain MEM, collected by centrifugation at 2000 rpm for 5 min; 5×10^6 cells were injected intraperitoneally in NOD/SCID mice for establishment of the PDXs. Tumor ascites formation was observed after 3 months, this was tapped, washed with PBS and injected into a new batch of mice. mAb150 treatments were administered to the 5th passage of PDX. In the initial experiments with A4 xenografts (Figs.1B-iv, -v), effects of mAb150 were evaluated in comparison with those of IgM isotype control (Sigma-Aldrich # M-5909). Limiting dilution assay was performed to evaluate tumor initiating potential. Briefly, tumor cells (5000, 10,000, or 20,000) were injected subcutaneously (1:1-matrigel: PBS) in NOD/SCID mice. Tumor formation was monitored for one month after injection.

Antigen localization and immunoblotting

Immunoblotting including preparation of whole cell protein lysates and subcellular fractions, protein denaturation, SDS-PAGE run, transfer and antibody probing followed by detection was performed as described earlier [15]. β-actin was used as internal control unless specified otherwise. Details of all antibodies used can be provided on request.

Immunoprecipitation

Whole cell proteins (A4) were prepared in RIPA (1 M Tris pH 7.4, 4 M NaCl, 0.5 M EDTA, NP-40, 10% SDS) buffer containing 1X protease inhibitor cocktail as described earlier [15]. Recombinant Anx1–12 proteins were used at 500 μg concentration. mAb150 antibody (5 μg/mg protein) was incubated overnight with whole cell proteins (input) with respective internal controls at 4 °C. Further, anti-IgM agarose (Sigma Aldrich, #324,374) beads were used for retrieval of antibody-linked proteins, as previously described [15]. For all experiments and wherever relevant, IgM isotype control (Sigma-Aldrich # M-5909) and bead controls were used.

Antigen identification by MS/MS sequencing

mAb150-immunoprecipitated proteins were resolved in 12.5% SDS-PAGE gel stained with mass-spectroscopy compatible Coomassie stain (Pierce, CA, USA). Individual protein bands (based on molecular weight) were excised, digested, desalted and purified for acquisition of spectra a 4800 MALDI-TOF/ TOF mass spectrometer (AB Sciex, Framingham, MA) and protein identification performed using MASCOT (version 2.1; http://www.martixscience.com) on search engine against the SwissProt database as described earlier [16].

Construction and expression of Anxa2 deletion mutants

AnxA2 protein was amplified using a cDNA clone (Origene RC205081) and cloned into the pGEX4T3 vector with a N-terminal GST tag. A series of 12 Anxa2 fragments (detailed in Fig. S4) were expressed in a similar manner. Protein expression was induced using 1 mM IPTG at 22 °C for 16 h. Expressed proteins were extracted and sonicated in lysis buffer containing 1 M Tris (pH 8.0), 300 mM NaCl, 0.1% TritonX-100, 2 mM PMSF and protease inhibitor cocktail (Roche). Lysate was clarified by centrifugation at 13,200 rpm at 4 °C for 30 min and the supernatant purified with GST-Sepharose beads (GE biosciences). Sequences of primers used for generation of these mutants are listed in Supplementary Data 2.

MTT assay for cytotoxicity/cell viability analysis

Cell viability on exposure to mAb150 (2–20 mg protein/ml), 5Aza-dC and CBB1007 (5 and 7 mmol respectively - standardised earlier) was assessed over 96 h using MTT assay. Following treatment, MTT (Sigma, 5 mg/ml) was added, and plate was incubated for 4 h at 37 °C in the dark. The insoluble formazan crystals were solubilized in acidified isopropanol and absorbance measured at 570 nm. Viability was calculated as a% ratio of test wells over the IgM isotype control (Sigma-Aldrich # M-5909). We further evaluated the neutralizing effects of mAb150, which revealed low IC_{50} values in high AnxA2-expressing cells and affirmed the high specificity of mAb150. Due to this specificity, a more accurate estimation of IC50 values would be the concentration required to reduce 50% of Anxa2 expressing cells in a population, which we termed as Anxa2 expression normalized IC50 (nIC50) values. Viability during in vitro migration assays was evaluated by treating cells with propidium iodide (200ug/ml) at specific time points after wound induction. Percent dead cells were quantified for thresholded phase-contrast and fluorescence images with the 'Analyze Particles' Plugin in the Fiji software.

FACS staining and resolution of various tumor cell fractions for clonogenicity and in vitro tumorigenicity

Resolution of the tumor regenerative hierarchy was based on a PKH label chase as described earlier [12, 17]. Briefly, freshly labeled PKH67 cells and unlabeled tumor cells were used before each acquisition of xenograft fractionation as positive and negative controls, along with propidium Iodide (PI) and Hoechst–Pyronin Y-stained cells. Each PKH-derived fraction was analyzed independently with PI and Hoechst–Pyronin Y-based DNA content and cell cycle analysis. Together, this identified 18 discrete tumor cell fractions which were analyzed and

assayed for Clonogenicity and in vitro tumorigenicity as described earlier [12]. Flow cytometry was performed on BD FACS Aria II Sorp (BD Biosciences, San Jose, CA, USA), and data analyzed using the BD FACS Diva 6.0. mAb150 treated xenografts along with age-matched controls were harvested as per experimental schedule and processed for FACS based quantification of 18 tumor fractions. For comparisons between cell lines, FACS sorted treated versus control cells were similarly considered. Log2 (fold-change of the percent frequencies of residual tumor fractions) following mAb150 treatment were normalized with those of corresponding control tumor fractions using Pearson's correlation distance matrix, average linkage methods and one-way hierarchical clustering based heatmap generated using MeV 4.8.1 (TM4 developer team, Boston, MA, USA). Functional clonogenicity assays were also performed and fold-change between control and mAb150-treated sets estimated.

Spheroid formation and immunostaining

5×10^4 sorted cells/well from each sorted tumor fraction were seeded in ultra-low attachment plate (Corning, Tewksbury, MA, USA) in MEM Medium containing 1% serum and incubated at 37 °C for 14 days before quantifying spheroids; images were captured on Olympus IX71 microscope (Dulles, VA, USA). For immunostaining, spheroids were fixed with 4% paraformaldehyde and stained with mAb150 (1:10,000 dilution) as described earlier [18].

Wound closure, cell invasion assays and migration mode (EMT, aCCM or pCCM) analysis

Wound closure and cell invasion assays along with the analysis for migratory mode determination were performed as previously reported [18].

Enzyme-linked immunosorbent assay (ELISA)

ELISA was performed using standard protocols. Briefly, 96-well plates were coated with the antigen (10μg/well) and incubated overnight at 4 °C. Each well was washed with ~200 μL wash buffer and incubated with 200 μL blocking buffer per well for 1 h at room temperature. 100 μL of standards and samples (in triplicate) were loaded in designated wells, incubated for 1 h at room temperature, washed 5 times with ~200 μL wash buffer. 100 μL of the antibody solution in blocking buffer (1:100) was added in each well, and incubated for 3 h at room temperature, washed 5 times with wash buffer and probed by adding streptavidin-HRP solution followed by TMB substrate solution. After adding stop solution, absorbance of each well at 450 nm was recorded with a plate reader. Data was normalized with that of IgM isotype control (Sigma-Aldrich # M-5909).

Semi-quantitative reverse transcription-PCR

Total RNA was isolated from cells using the Qiagen RNeasy minikit (Qiagen, Inc.) according to the manufacturer's protocol and semi-quantitative reverse transcription-PCR was performed under standard conditions as described previously [19]. Amplified products were resolved on a 1.5% agarose gel; GAPDH was used as internal control. Details of primer sequences are listed in Supplementary Data 3.

Immunohistochemistry (IHC)

IHC was performed on xenografts as described earlier [20]. Briefly, 5 μm sections were fixed at 60 °C for 1 h, deparaffinized in xylene, hydrated in ethanol-distilled water gradient and incubated for 30 min at pH 6 for heat-induced epitope retrieval (HIER). Peroxidase inactivation was performed by incubating sections in 3% H_2O_2 for 30 min (Qualigens, MA, USA), followed by 1x Blocking Solution for 10 min (Biogenex, CA, USA) and overnight incubation in primary antibody. Sections were washed, incubated with anti-rabbit HRP-conjugate (Jackson Laboratories, Inc., PA, USA) for 1 h, and color developed with DAB (Thermo Pierce, MA, USA); hematoxylin was used as a counterstain. Dehydrated sections were mounted in DPX (Qualigens, MA, USA). For all experiments either IgM isotype (Sigma-Aldrich # M-5909) or controls without primary antibody were used.

Prediction of binding epitope for Anxa2

The sequence of AnxA2 was retrieved from UniProtKB - P07355, and its complete structure was prepared using two entries from Protein Data Bank – 1W7B and 4FTG. Five different prediction platform/servers were used for the prediction of AnxA2 epitopes – ABCpred, BepiPred-2.0, FBCPred, BCPred and Ellipro [21–24]. The part of protein sequence that was predicted as an output by all the five servers was considered as potential epitope region, sequences predicted by 4 out of 5 servers were processed.

Statistical analysis

Unless mentioned otherwise, all experiments were carried out at least in triplicate. Results are expressed as mean ± *S*.E.M. of 3 independent experiments. Significant difference of mean values determined using two-tailed Student's t-test (SigmaStat software; $^*P<0.05$; $^{**}P<0.01$; $^{***}P<0.001$).

Results

mAb150 development and identification of an immunogenic target protein

A secretory hybridoma clone was developed by fusion of SP2/0 myeloma cells with Balb/c mouse spleen-derived B cells previously primed with cell membrane proteins of an ovarian cancer stem-like cell line (A4; {Bapat, 2005 #35}; S.Data1;Fig.S1). The antibody secreted by this clone was isotyped as IgM kappa and designated mAb150. Immunoblotting of A4 cell lysates identified a 29–37 kDa protein as the antigen recognized by mAb150 (Fig. 1A-i). Tryptic digestion of mAb150-immunoprecipitated protein, consequently sequenced by MALDI-TOF applying probablity-based mowse score with rational peptide sequence coverage and lower RMS identified human AnxA2 as the target protein (S.Data2;Fig.S2). Further validation was performed by probing either mAb150 immunoprecipitated (i) A4 cell lysates or (ii) purified commercial AnxA2 protein (Origene TP305081) with mab150 and commercial Annexin A2 antibody (sc-28,385) (Figs.1A-ii-v). The target protein was localized in membrane, cytoplasmic and nuclear fractions of A4 cell lysates (Figs.1A-vi, viii). Importantly, expression of AnxA2 in A4 cells (Figs.1B-i-ii) correlated with growth inhibition by mAb150 as revealed in MTT assays (IC_{50}–10μg). A significant reduction of A4 xenograft volumes in mice treated with mAb150 (Figs.1B-iii-iv) was associated with a depletion of Anxa2 expressing cells thus, highlighting the target specificity of this neutralizing antibody (Fig.1B-v).

mAb150 neutralizing effect correlates with Anxa2 expression in tumors

Profiling surface expression of AnxA2 across a panel of 24 cancer cell lines (representing 9 different tumor types including ovarian, breast, prostate, colon, glioblastoma, lung, kidney, skin, and cervical cancer) revealed a cell system specific range of expression (14%–61.5%; Tables S1-S2). We further evaluated the neutralizing effects of mAb150, which revealed its low IC_{50} values in high AnxA2-expressing cells and affirmed the high specificity of mAb150. Due to this specificity, a more accurate estimation of IC50 values would be the concentration required to reduce 50% of Anxa2 expressing cells in a population, which we termed as Anxa2 expression normalized IC50. This is important since it would also provide a more accurate comparison of mAb150 efficacy

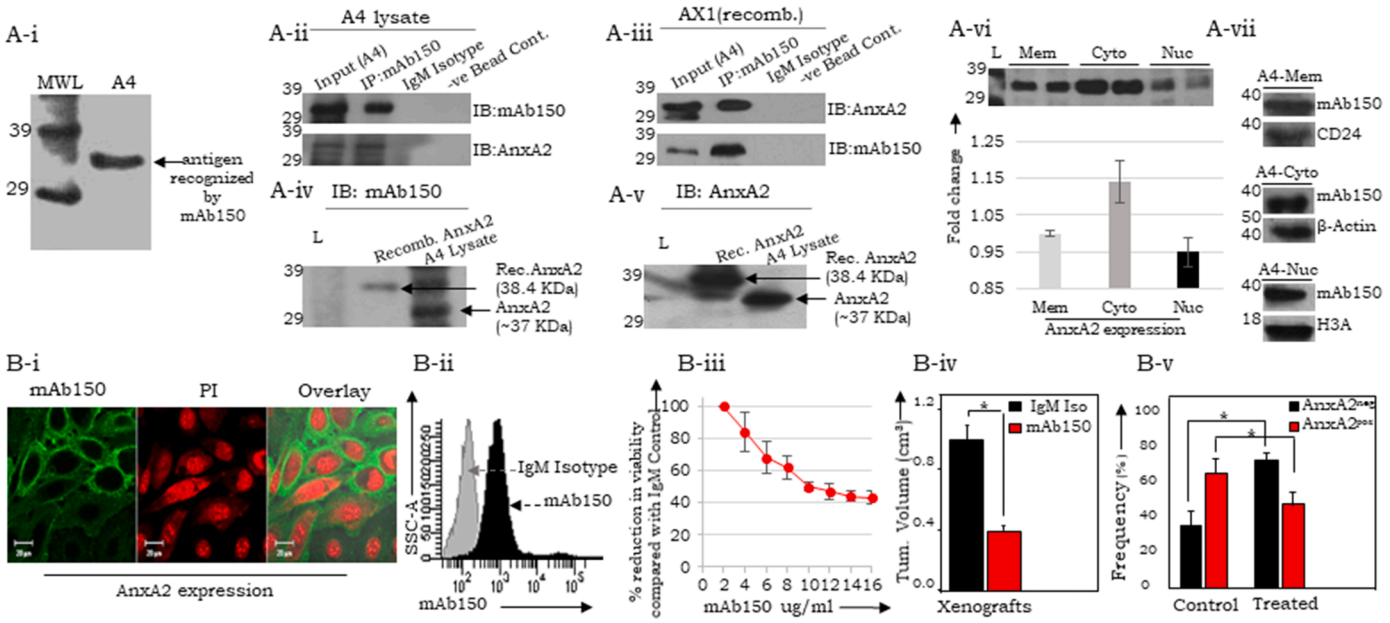

Fig. 1. Target identification, localization, and specificity of mAb150 in A4 cells. A-i. Immunoblotting of A4 whole cell lysates with mAb150; A-ii,A-iii. Cross-immunoprecipitation (IP) followed by probing of A4 lysate and Ax1 protein with mAb150 and commercial AnxA2 antibody and relevant controls; A-iv, A-v. Representative IB of mAb150 and commercial AnxA2 antibody with pure human recombinant Anxa2 protein and A4 lysates; A-vi, Avii. Localization of mAb150 target across membrane (Mem), cytoplasm (Cyto) and nuclear (Nuc) subcellular fractions (CD24, B-actin and H3A are respective controls) in A4 cells; B-i, ii. Anxa2 expression profiling through immunofluorescence staining and flow cytometry respectively; B-iii, B-iv. Cytotoxicity of mAb150 in A4 cells (MTT) and xenografts respectively; B-v. Significant reduction of AnxA2 expressing tumor cells following six doses of mAb150 treatment (18 mg/Kg) with 4 days of recovery between consecutive doses. For all experiments and wherever relevant, IgM isotype control (Sigma-Aldrich # M-5909) was used. *$P<0.05$; **$P<0.01$; ***$P<0.001$.

across a panel of cancer cell lines representing different tumor types with intrinsically different expression of Anxa2. Thus, normalized IC_{50} values (nIC_{50}) ranged between 12.04–172.9 μg/ml across the panel of cell lines tested (Fig. 2A), indicating differential efficacies of mAb150, being highest in glioma (U373) xenografts and lower in lung adenocarcinoma (A549) (Fig.S3A).

Tumor regression was associated with reduced AnxA2 expression (maximal reduction in ovarian, A4 and least in cervical, ME180 xenografts). Derivation of nIC_{50} values in xenografts demarcated two response groups, 'Group a' (low AnxA2 expression, low mAb150 efficacy - OVCAR3, ME180, A549) and 'Group b' (high AnxA2 expression, high mAb150 efficacy and regression - A4, MCF7, A431, PC3, HT29, U373; Fig.2B; Table S3; Fig.S3). These data affirmed direct correlation between AnxA2 expression and mAb150 efficacy. Such specificity further led us to explore the modulation of AnxA2 expression by epigenetic drugs to reverse promoter methylation as reported earlier [12]. Treatment of A4 and OVCAR3 cell lines with a combination of mAb150 with either a demethylating agent (5-Aza-Dc; 5 mM) or HMATase inhibitor (7 mmol) significantly increased AnxA2 expression and reduced cell growth (Figs.2C-D). This data suggests epigenetic potentiation could complement targeting of tumor cells by mAb150.

Determination of mAb150 binding epitope across the Anxa2 protein sequence

To identify the specific human Anxa2 epitope targeted by mAb150 we performed sequential linear epitope prediction with publicly available algorithms (UniProtKB P07355; [22]). A higher epitope propensity spanning residues 4–41 at the N-terminal region of AnxA2 was thus predicted (Table S4). This linear prediction was validated by screening differential binding of mAb150 to peptide fragments representing distinct stretches of amino acids across the entire AnxA2 sequence (Ax1 to Ax12; Figs.S4). This indicated maximal affinity of mAb150 towards Ax1 (Full length), Ax2 (Residues 1–169), Ax4 (Residues 1–113) and Ax7 (Residues 1–50) fragments, all of which contain the N-terminal region of AnxA2 (Figs.3A-B,3E; anti-GST tag used as control). Immunoprecipitation of Ax4, Ax5, Ax6, peptide fragments with mAb150 revealed preferential binding for Ax4 and further with Ax7 (Figs.3C-E), which was confirmed through ELISA (Fig. 3F).

Final validation of the predicted mAb150 linear epitope was achieved through ELISA by using synthetic, non-overlapping 10-mer peptides covering amino acids 1–113 of the AnxA2 sequence (AP1-AP11). This revealed highest affinity of mAb150 for residues 11–20 (AP2) (Fig.3G-i; commercial AnxA2 antibody sc-166,762 recognizing C-terminal epitope (region covering 324–339 residues) was used as negative control (Fig.3G-ii). Overall, these experiments confirmed that mAb150 preferentially recognizes an epitope involving the N-terminal amino acids 11–20.

We further mapped AnxA2 epitopes at atomic resolution by applying a 3D structure-based epitope prediction platform (Ellipro) and artificial intelligence (AI)-based prediction platform/servers (ABCpred, BepiPred-2.0, FBCPred, BCPred) that compute from knowledge-based B-cell epitopes/non-epitopic datasets. Mapping of AnxA2 N-terminal 1–50 aa input sequence predicted a common epitope across all 5 platforms, the core of which comprised residues 16–21 further corroborating with the immunoreactivity observed between mAb150 and AP2 peptide (11–20 aa;Figs.3G-i;Figs.3Hi-ii). Molecular representation positioned this epitope on the surface of Anxa2 which suggests the feasibility of mAb150 binding to the folded protein (Figs.3H-iii, Fig.S5A). Similar mapping of full-length AnxA2 linear sequence did not qualify any potential epitopes across all 5 platforms, except a minor core overlapping sequence between 145 and 170 aa position (Fig.S5B). These results demonstrated the presence of a dominant and most favored immunogenic AnxA2 epitope in proximity of its N-terminal.

AnxA2 expression networks and protein interactions assign a context of involvement in active migratory modes but not in passive collective cell migration

To identify the molecular interactors of Anxa2 which facilitate its functions in cancer cells, we immunoprecipitated AnxA2-bound proteins in A4 cell lysates with mAb150 and followed it up with MS/MS. This

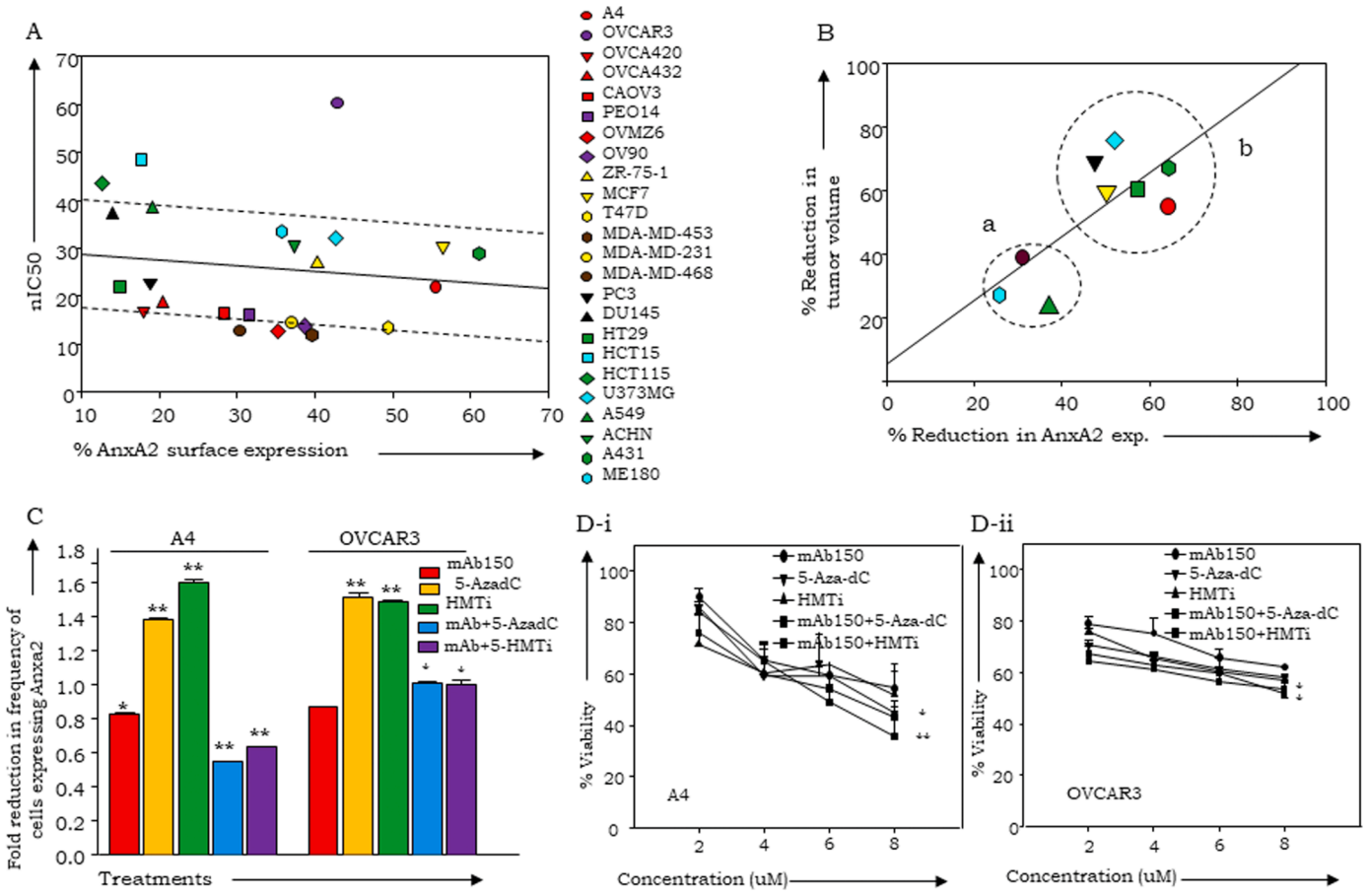

Fig. 2. Correlation of AnxA2 expression with mAb150 cytotoxicity and epigenetic potentiation. A. Normalized IC50 values (nIC_{50}) of mAb150 in cell lines; B. Correlation between reduction in AnxA2 expression and xenograft regression following mAb150 treatment segregates two clusters, Group a: low AnxA2 expression-low efficacy, Group b: high AnxA2 expression-high efficacy; C, D. Epigenetic potentiation for mAb treatment in terms of enhanced AnxA2 expression after individual and combined treatment with epigenetic drugs 5-Aza-dC or HMTase inhibitor (5 mM and 7 mmol respectively) in A4 (C, D-i) and OVCAR3 (C, D-ii) cells; $^{*}P<0.05$; $^{**}P<0.01$; $^{***}P<0.001$.

revealed α-enolase (ENO1), pre-mRNA splicing factor (SF2), Gelsolin (GSN) and histones H2A, H3, H4 as interacting partners of AnxA2 (Fig. 4A; [12,25]). Assessment of genes co-expressed with AnxA2 in The Cancer Genome Atlas (TCGA Agilent platform; 598 tumor samples) ovarian cancer dataset identified 4 strong positively correlated genes (0.5>R2<−0.5) viz. PLAU, PMP22, EMP1, and S100A10 which were validated in A4 cells (Figs.4B-C). Relaxing the threshold (0.35>R2<−0.35) further identified 291 positively correlating genes including those associated with the extracellular matrix (ECM) and epithelial to mesenchymal transition (EMT) viz., COL11A1, COL6A2, COL6A3, COL5A1, COLA1A, FBN1, SPARC, FN1, COL5A2, VCAN, THBS2, ITGA11, MMP2, SNAI2, FAP (Fig.4D). Due to the association of these processes with cancer metastasis we explored the effects of mAb150 in possibly inhibiting metastasis. We observed that treatment with mAb150 severely diminished migratory and invasive properties of A4 cells as compared to untreated controls (Figs.S7A, S7B, S7C). To some extent, the reduced migratory capabilities may be also be attributed to the cytotoxic effects of mAb150 as is evident through membrane damage and nuclear fragmentation in A4 cells (Figs.S7D) and further substantiated as reduced cell viabilility during wound healing (S7E).

We further investigated the differential association of AnxA2 correlating genes in ovarian cell lines with a mesenchymal (A4, CP70) vs. epithelial (OVCAR3, OAW42) phenotype. ANXA2, EMP1, PMP22, S100A10, PLAU, SF2 and GSN transcripts were expressed at higher levels in mesenchymal cells affirming their functional correlation with EMT; consequently, lower expression of SNAI2, DCN, FAP, FN, FBN1, SPARC, LOXL2 and S100A10 was evident in cell lines with an epithelial morphology (Figs.S8A-B). This affirmed an association of AnxA2 with a mesenchymal phenotype (Fig.S8C). These observations were further supported with an evaluation of the three discrete modes of migration (EMT, aCCM – sheet/active collective cell migration and pCCM - passive collective cell migration) that we previously identified in a panel of ovarian cancer cell lines. The latter included epithelial (E-OVCAR3), intermediate epithelial (iE-CAOV3), epithelial-mesenchymal hybrid (E/M-PEO14), intermediate mesenchymal (iM-A4) and mesenchymal (M-OVMZ60) phenotypes represented in the corresponding cell lines [10]. Interestingly, the cytotoxic activity of mAb150 displayed a gradient of decreasing efficacies from the mesenchymal to epithelial phenotypes; OVMZ6 (nIC50:18μg), A4 (nIC50:19.5μg), PEO14 (nIC50:25.6μg), CAOV3 (nIC50:29.0μg) to the lowest for OVCAR3 (nIC50:70μg). In live wound healing imaging assays, A4 cell migration was maximally restricted by mAb150 treatment, followed by CAOV3 and OVMZ6, while OVCAR3 cells were possibly refractory due to their inability to actively migrate into the open wound area (Fig.4E; Supplementary Videos S1-S4). The mean velocity of migration was significantly hampered after mAb150 treatment of PEO14, A4 and OVMZ6 cells (Fig.4F). Subsequent analysis of nearest neighbors and migration trajectories identified a shift towards the aCCM mode of migration in A4, OVMZ6 and PEO14 cells as previously reported ([10]; Figs.S9A, S9B). Cumulative evaluation of mAb150 efficacy on cell migration was obtained by superimposition all these parameters through Principal Component (PC) analysis using quantifiable metrics of cell displacement (Final Y), velocity and nearest neighbors which affirmed strong responsiveness of OVMZ6, A4 and PEO14 cells to mAb150 treatment (Fig.4G). Conclusively, this suggests a

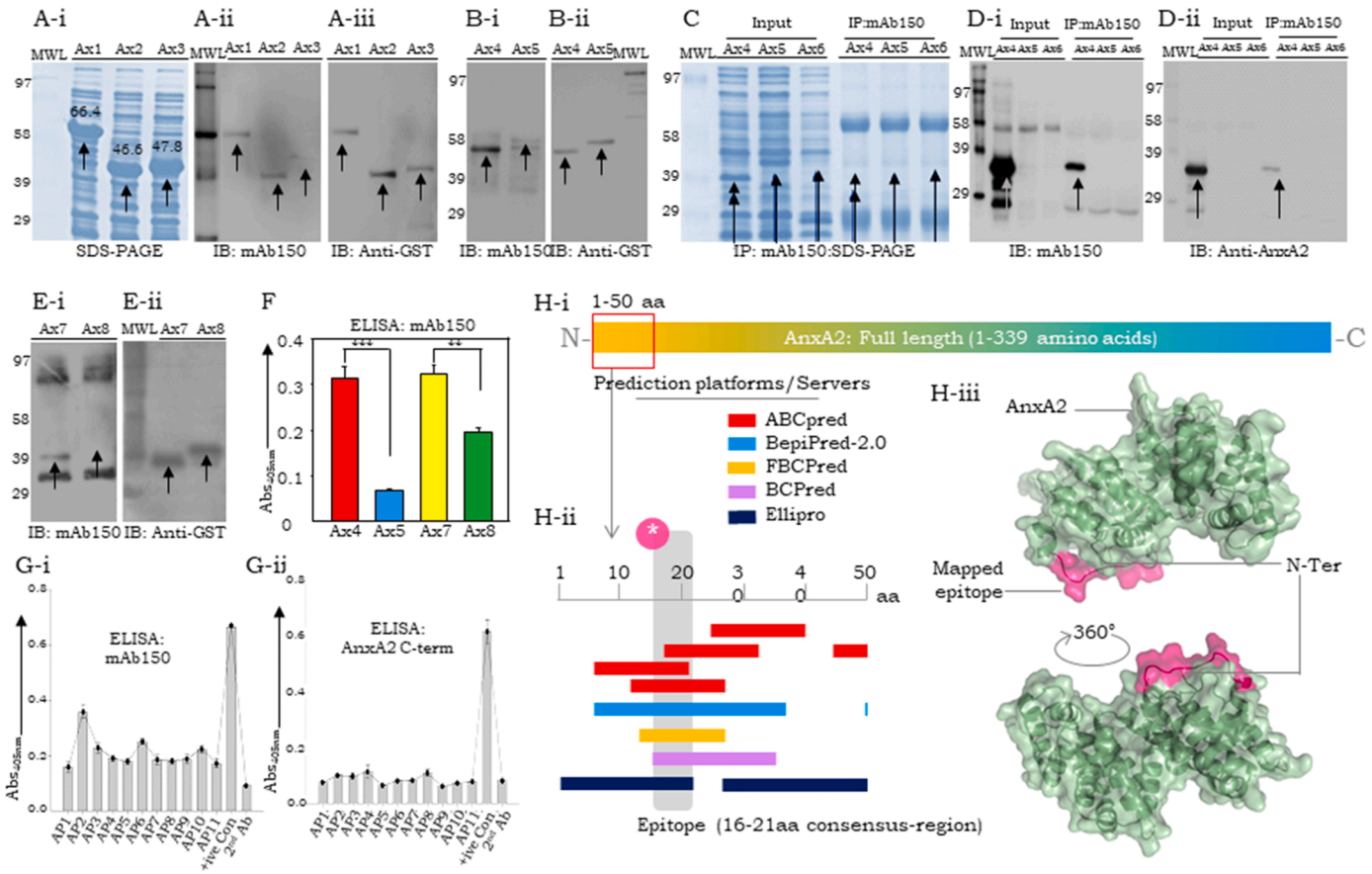

Fig. 3. Determination of mAb150 reactive epitope. A-i. Coomassie blue stained SDS-PAGE protein gel of recombinant protein lysates of Ax1, Ax2 and Ax3, A-ii. Immunoblotting of Ax1, Ax2 and Ax3 recombinant lysates probed with mAb150 and consequently with Anti-GST (A-iii); B-i. Immunoblotting of Ax4 and Ax5 recombinant lysates probed with mAb150 and consequently with Anti-GST (B-ii); C. Coomassie blue stained SDS-PAGE protein gel of recombinant protein lysates of Ax4, Ax5 and Ax6 (left panel) and immunoprecipitated with mAb150 (right panel), followed by immunoblotting with mAb150 (D-i) and Anti-Anxa2 (D-ii); E. Immunoblotting of recombinant protein lysates of Ax7 and Ax8 with mAb150 (E-i) and Anti-GST(E-ii); F. ELISA-based profiling of mAb150 reactivity with Ax4, Ax5, Ax7 and Ax8 fragments; G. ELISA-based profiling of reactivity with synthetic peptides Ap1-Ap12 of (G-i) mAb150, and (G-ii) commercial AnxA2 C-terminal antibody (sc-166,762); H-i. Mapping of mAb150 epitope on AnxA2 1–50 aa sequence by 5 different servers, indicating (H-ii) overlapping epitope region (annotated by different color lines) in proximity of the N-terminal region (a core overlapping epitope is highlighted by gray background, annotated as *), (H-iii). Molecular surface view model that indicates its location (marked in pink) on the AnxA2 protein (green).

functional involvement of AnxA2 in active cell migration (aCCM and EMT) since mAb150 treatment maximally affected cells which migrated through these modes.

Determination of cellular targets of mAb150 in xenograft tumors indicates minimal regenerative potential following mAb150 treatment

While xenograft regression indicated specific targeting of AnxA2 expressing cells, it did not reveal the extent of regenerative potential of residual tumor cells which evade treatment. To address this issue, we applied a previously established 3-level flow cytometry-based approach that resolves and identifies enriched populations in xenograft tumors following mAb150 treatment ([12,17]; S.Data 4; Figs.5Ai-5Aii). Briefly -

i Label-chase of vital lipophilic membrane dye, PKH67 in xenografts resolved the proliferative hierarchy (Fig. 5-Aiii-top panel). Quiescent CSCs associated with maximal regeneration resided in PKH^{hi}, progenitors in PKH^{lo} and differentiated cells in PKH^{neg} fractions. mAb150 treatment led to significant reduction of the PKH^{hi} fraction in A4, OVCAR3, PC3, MCF7, ME180, U373, A549, A431 xenografts (Fig.5B-i).

ii Propidium iodide (PI) - based DNA content analysis identifies host (mouse), euploid and aneuploid tumor cells in xenografts (Fig.5A-iii-middle panel). mAb150 treatment led to decreased host and euploid fractions in xenografts (Fig.5B-ii).

iii Hoechst-Pyronin Y staining-based DNA-RNA content analysis along with PI staining resolves cell cycle phases (notably segregation of G0 from G1) within ploidy-based fractions (Fig.5Aiii-bottom panel). Significant reduction of Euploid G0 concurrently with increased Euploid G1 cells was evident in mAb150 treated A4 xenografts, while in other xenografts both fractions were reduced (Fig.5B-iii).

Sorting of the various A4 xenograft cell fractions was performed to evaluate residual regenerative potential following mAb150 treatment (3 doses, 150 μg protein/site for 2 weeks followed by 1 week of recovery). Capabilities of regenerating suspended spheroids, adherent colonies, anchorage independent colonies in soft agar and migration to mediate wound healing were significantly reduced after mAb150 treatment especially in the PKH^{hi} and PKH^{lo} cells (Figs.5C-i-iv). Limiting dilution assays further indicated that following either a 3-dose (3D) or 6-dose therapeutic regimen of mAb150, residual tumor regenerative potential is maximal in the PKH^{hi} euploid fractions that could be assigned a significant tumor initiating frequency, while a much higher number of PKH^{lo} euploid cells are required to regenerate tumors following treatment, and PKH^{neg} cells failed to generate any tumors (Figs.5D-i, D-ii).

Further, mapping AnxA2 expression onto these fractions identified differential responses of AnxA2^{pos} and AnxA2^{neg} populations within A4 xenografts (Fig. 6A-i). AnxA2^{pos} regenerative hierarchy and aneuploidy cells were directly targeted by mAb150 (Fig.6A-ii), while an increased

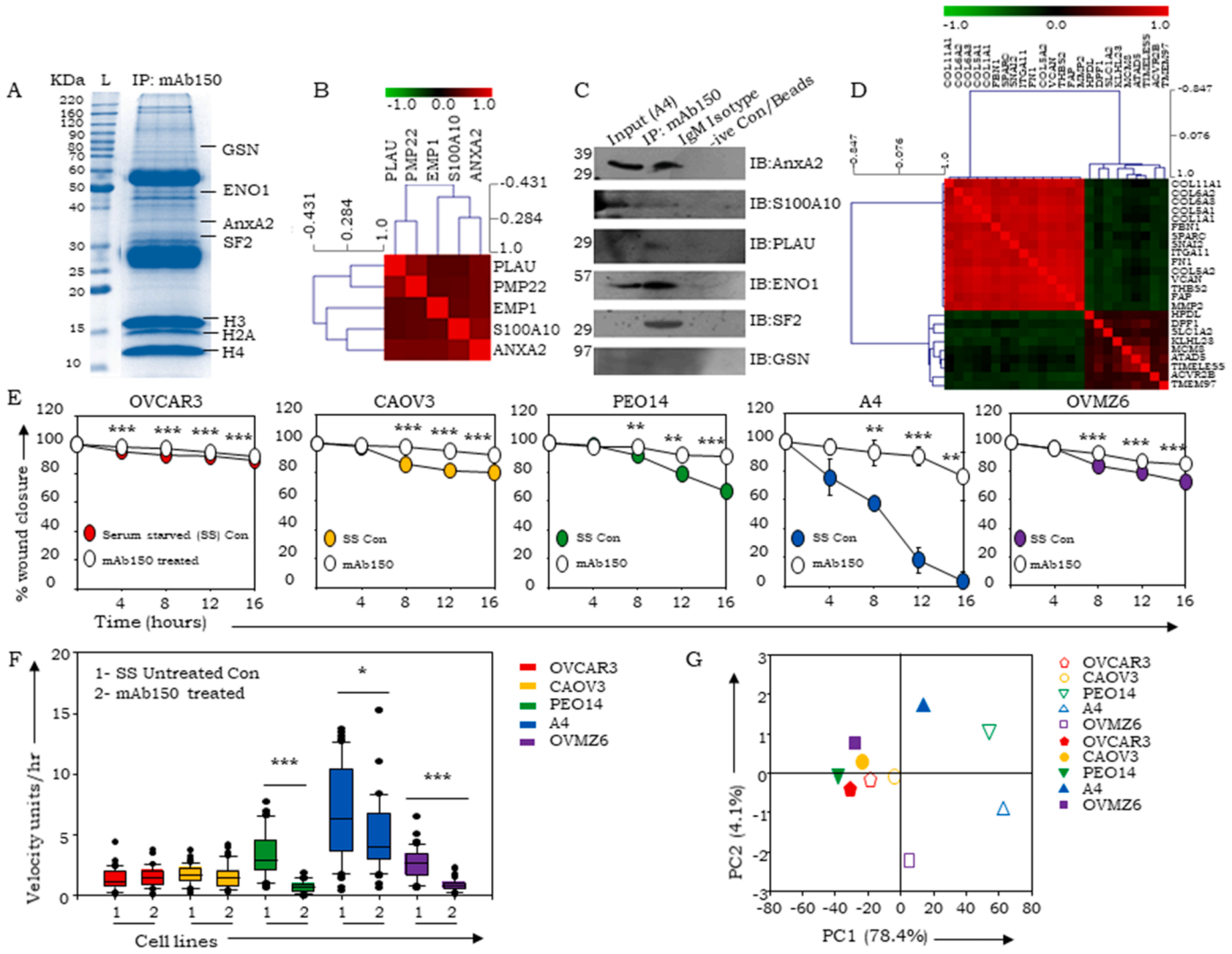

Fig. 4. Identification of interacting partners and co-expression network towards functional evaluation of AnxA2. A. Representative mAb150 immunoprecipitated proteins stained with Coomassie Blue; B. Correlation plot for positive correlating genes with ANXA2 gene expression in HGSC-TCGA dataset; C. Validation of predicted and immunoprecipitated AnxA2 correlating proteins by immunoblotting; D. Plot indicating correlation between EMT signature AnxA2 hub genes; E. Representative migration capabilities estimated as percent in vitro open wound area for OVCAR3, CAOV3, PEO14, A4 and OVMZ6 cells following mAb150 exposure, serum starved (denoted by ss) cells used as control; F. Representative box plots of mean migratory velocity (pixels/hr) comparison between 1: Control (Serum starved) and 2: mAb150 treated cells; G. Principal component (PC) analysis of time-lapse imaging-based migration data of control and mAb150 treated cells, filled and empty shapes indicate control and mAb150 treated cells respectively. *$P<0.05$; **$P<0.01$; ***$P<0.001$.

G0 fraction in AnxA2^{neg} cells suggested likelihood of progenitors entering quiescence (possibly tumor dormancy); drug refractory proliferative cells were localized in the euploid fraction (Figs.6A-iii-iv). Residual regenerative potential was majorly seen in cells of the AnxA2^{neg} fraction, with a few AnxA2^{pos} cells (likely to be drug resistant) retained in vitro spheroid, adherant and soft agar colony formation capabilities (Figs.6B-i-ii). Such residual functionality was also observed in other tumor xenografts (Figs.6C-i-iii). Conclusively, resolution of intra-tumor cell heterogeneity and differential AnxA2 expression identified specific fractions that may either be sensitive, refractory, or resistant to mAb150 treatment.

We combined all three levels of resolution to compute an 18-cell population 'tumor cytotype' that strengthens drug evaluation vis-à-vis prediction of residual regenerative potential within tumors (Fig.S6A; [12,25]). mAb150 treatment perturbed the tumor cytotype by targeting all sub-populations of the PKH^{hi}, PKH^{lo} and host fractions. A striking observation was of possible re-entry into the cell cycle of the otherwise dormant G_0-PKH^{hi} cells (Fig.S6B-inset). A comparative pan-cancer analysis indicated similar patterns of responses in all xenografts, wherein targeting of PKH^{hi} fraction was associated with emergence of cycling populations; surprisingly the PKH^{neg} fraction was better targeted in OVCAR3, A431, PC3, A549, ME180 and U373 xenografts (Fig.S6C). Profiling of AnxA2 expression within this cytotype affirmed reduced frequency of all AnxA2^{pos} fractions following treatment, accompanied by an increased cycling of residual AnxA2^{pos} and AnxA2^{neg} PKH^{hi} populations (Fig.S6D). Concurrently, in the AnxA2^{neg} fraction, while PKH^{neg} cells were reduced following treatment, PKH^{lo} cells were increased following mAb150 treatment (Figs.S6E-i-ii). The common feature across all tumors following treatment with mAb150 was the emergence of cycling CSC populations. However, those in the AnxA2^{neg} fraction are indicated to have lower regenerative potential (most progenitor sub-populations are arrested at G1-S) than in the AnxA2^{pos} fraction. This profiling provided an additional dimension of differential cycling as an end-point measure of residual regenerative potential, besides affirming the target specificity of mAb150 across cancer types.

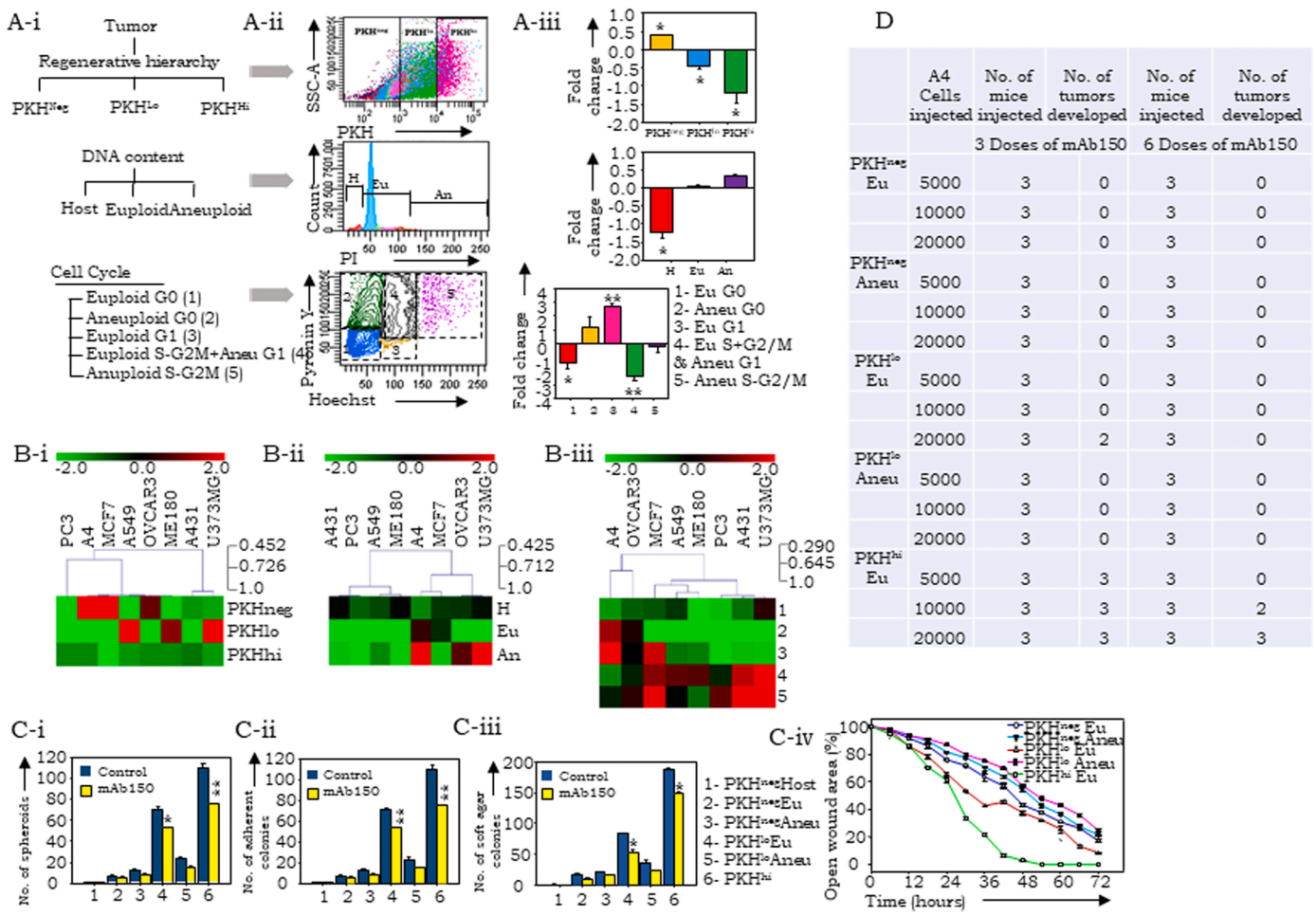

D

	A4 Cells injected	No. of mice injected	No. of tumors developed	No. of mice injected	No. of tumors developed
		3 Doses of mAb150		6 Doses of mAb150	
PKH^{neg} Eu	5000	3	0	3	0
	10000	3	0	3	0
	20000	3	0	3	0
PKH^{neg} Aneu	5000	3	0	3	0
	10000	3	0	3	0
	20000	3	0	3	0
PKH^{lo} Eu	5000	3	0	3	0
	10000	3	0	3	0
	20000	3	2	3	0
PKH^{lo} Aneu	5000	3	0	3	0
	10000	3	0	3	0
	20000	3	0	3	0
PKH^{hi} Eu	5000	3	3	3	0
	10000	3	3	3	2
	20000	3	3	3	3

Fig. 5. Evaluation of mAb150 efficacy in A4 xenograft cell sub-populations following treatment (3 doses, 18 mg/kg; 1-week recovery between and after doses). A-i, ii. Schematic and corresponding dot blots in flow cytometry data for resolution of cell fractions- Top panel: label-chase identifies Pkh^{hi} (CSCs), PKH^{lo} (progenitors and aneuploid cells), PKH^{neg} (differentiated cells). Middle panel: PI based-DNA content resolves Host, Euploid and Aneuploid populations. Lower panel: Hoechst-Pyronin Y-PI based DNA-RNA quantification resolves 5 fractions viz. 1: Euploid G0, 2: Aneuploid G0, 3: Euploid G1, 4: Euploid S-G2/M and Aneuploid G1, 5: Aneuploid *S* – G2/M populations, A-iii. Fold-reduction following mAb150 treatment of the cell populations described in 3A-i; B. Heatmap representations of consolidated fold-change in the frequency of individual fractions between 8 treated xenografts and appropriate controls across - i. PKH regenerative hierarchy-based, ii. Ploidy-based and, iii. Ploidy-Cell cycle phase-based fractions; C. Evaluation of residual regeneration in mAb150 treated A4 xenografts assayed for- i. spheroid formation, ii. adherent colony formation, iii. soft agar colony formation, iv. Wound healing assay; D. Limiting dilution assays (3D – 3 doses of mAb150, 6D – 6 doses of mAb150 as described in methods), i. Tumor regenerative potential 0f 5000, 10,000 and 20,000 residual cells of sorted fractions, ii. Tumor initiating frequencies of residual cells of sorted fractions. 1:PKH^{neg}Host, 2:PKH^{neg}Eu, 3:PKH^{neg}Aneu, 4:PKH^{lo}Eu, 5:PKH^{lo}Aneu, 6:PKH^{hi}. *P<0.05; **P<0.01; ***P<0.001.

mAb150 prolongs tumor ascites formation and survival in a PDX model of ovarian cancer

Finally, we evaluated mAb150 efficacy in a Patient Derived Xenograft (PDX) model established using ovarian ascites derived from a patient with recurrent high-grade serous ovarian adenocarcinoma {data unpublished}. High AnxA2 expression was noted in peritoneal tumor ascites cells and multilayer spheroids developed in this model (Figs. S10A-B). Development of tumor ascites was delayed on administering 6 intraperitoneal doses of mAb150 to 35 days in this model from 21 days in vehicle treated control mice (Fig.S10C). Correspondingly, survival of mAb150 treated mice was extended from ~ 81 days (in vehicle treated controls) to 110 days (Fig.S10D). To further the effect of combination therapy, PDX mice were treated with 6 cycles of Paclitaxel (25 mg/Kg) monotherapy in combination with mAb150 (18 mg/Kg). This not only enhanced survival, but also the quality of life of mice since a reduced volume of peritoneal tumor ascites harbouring fewer number of tumor spheroids were observed under the treatment regime (Fig.S10E). This makes it pertinent to further evaluate other drug combinations with mAb150 towards improved treatment strategies and possibly achieve remission.

Discussion

Lack of target specificity and emerging resistance to chemotherapy has advocated for antibody-based therapeutic regimes in several malignancies, especially advanced-stage metastatic cancers. In the present study, we applied these principles to evaluate the efficacy of a monoclonal antibody developed in our lab. Identification of membrane bound AnxA2 as the target of mAb150 is suggestive of high antigenicity of the protein. The epitope recognized by mAb150 was localized to the AnxA2 N-terminal region (residues 11–20), which is crucial for its membrane localization and protein-protein interactions [9,26]. Of the multiple post-translational modifications reported in this region tyrosine 23 phosphorylation is known to promote EMT in pancreatic cancer [27–29]. A p11-dependent membrane translocation event is identified in this event, while phosphorylation is mediated via a feedback loop mechanism at the membrane [26–28]. AnxA2 usually functions with its partner S100A10 as a mono-/ hetero-tetramer [26]. The heterotetramer interacts with tissue plasminogen activator to facilitate conversion of

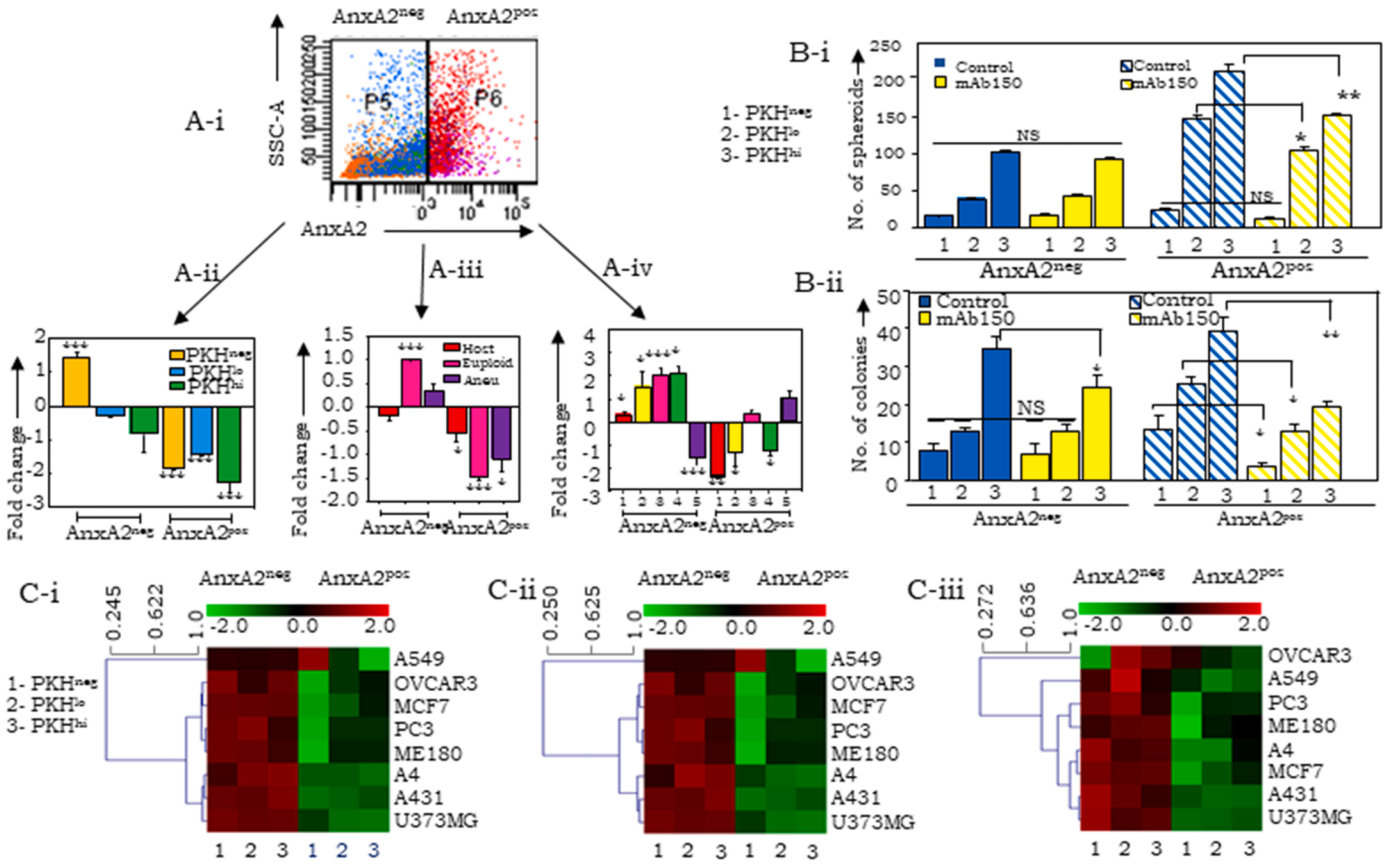

Fig. 6. Effect of mAb150 treatment on A4 xenografts vis-à-vis drug target (AnxA2) expression and altered fold-change in the respective, sorted tumor fractions following treatment. A-i. Schematic of AnxA2^{neg} and AnxA2^{pos} cell fractions in A4 xenografts; A-ii. Regenerative hierarchy, A-iii. Ploidy, A-iv. Cell cycle fractions; B. Comparison functional assays for capability to form spheroids (B-i) and soft agar colonies (B-ii) of the regenerative hierarchies in AnxA2^{neg} and AnxA2^{pos} cell fractions; C. Heatmap representation of C-i. Spheroid formation, C-ii. adherent colony formation and C-iii. soft agar colony formation capability of residual cells in each of the PKH regenerative hierarchy fractions across 8 tumor types (1:PKH^{neg}; 2:PKH^{lo}; 3:PKH^{hi}). NS- Not Significant. 1: Euploid G0, 2: Aneuploid G0, 3: Euploid G1, 4: Euploid S + G2/M and Aneuploid G1, 5: Aneuploid S − G2/M. *P<0.05; **P<0.01; ***P<0.001.

plasminogen to plasmin that leads to fibrinolysis [27]. It also regulates membrane dynamics during endocytosis-exocytosis and membrane trafficking, besides participating in EMT [30]. Inhibition of these interactions by synthetic peptides, immunotherapeutic agents, siRNA or aptamers abolish membrane localization and restrict cancer progression [30–35]. Elevated levels of AnxA2 in tumors correlate with drug resistance and poor prognosis in multiple metastatic tumors including renal, pancreatic, liver, urothelial, and lung cancers [36–39] (https://www.proteinatlas.org/ENSG00000182718-ANXA2/pathology). As a secretory protein, circulatory AnxA2 levels are reported to be elevated in metastatic hepatocellular and breast cancers [40].

The outcome of mAb150-mediated targeting of AnxA2 was similar to the earlier results obtained from multiple AnxA2-inhibitory approaches. The efficacy of mAb150 treatment across a panel of cancer cell lines and xenografts directly correlated with AnxA2 expression, which was reflected by lower IC50 values in AnxA2-high cells along with a high specificity in blocking its target. Given the fact that the mAb150-specific epitope lies within a functionally important region of the molecule, we anticipated and established that mAb150 treatment adversely affected the metastases-promoting functions of AnxA2. Analysis of AnxA2 expression networks and interactors indeed identified multiple co-expression partners of key EMT genes/modulators that were further validated. Tumor cells expressing AnxA2 were targeted by mAb150, and the treatment led to delayed migration through the aCCM and EMT modes, besides invasion. This assigns a cell phenotype-based context to the efficacy of Anxa2 inhibition, which is a novel feature of the present study. We additionally report that epigenetic potentiation of AnXA2 by 5-Aza-dC or HMATi in combination with mAb150 improved the efficacy of mAb150 and may deliver further prognostic benefits as is reported in immunotherapy [41,42]. Therapeutic relevance of mAb150 was finally affirmed through findings in PDX models in which formation of ascites/intraperitoneal spheroids (marked by high AnxA2 levels) were significantly delayed along with extended survival in treated mice.

Several preclinical cancer drug candidates often fall short of achieving therapeutic success and revoke remission. This is partly attributed to a lack of cytotoxicity end-point assays to identify drug-responsive cell fractions and map residual regenerative potential within treated tumors. Our earlier resolution of the heterogeneity of tumor cell populations and drug target expression determines responsiveness through multi-dimensional evaluation of a new drug candidate or combination, with due consideration of the drug refractory populations within tumors [12]. On evaluating the efficacy of mAb150 on this platform, treatment was seen to significantly reduce the frequency of quiescent CSCs and progenitor subsets. This seemed to be a two-pronged attack, specific targeting due to high expression of AnxA2 in these cells that leads to reduced clonogenicity, along with re-entry of the quiescent populations into the cell cycle that make them more vulnerable to drug targeting. AnxA2 is reported to be co-expressed with CSC markers including DCLK1, LGR5, and CD44 on circulating CSCs in clinical samples [43], suggesting AnxA2 expression in these populations made them vulnerable to mAb150 neutralizing activity. A similar mechanism was recently validated in prostate tumors where mAbs for angiogenin and plexin-B2 sensitized CSCs for chemotherapy by diminishing their stemness features [44]. Such sensitization could drive

exhaustion of the CSC-progenitor repertoire in xenografts, which reflects on the ability of mAb150 to perturb tumor heterogeneity by targeting regenerative sub-populations in tumors. Thereby, mAb150-driven AnxA2 neutralization could be an effective strategy for tumor regression and block disease relapse, especially in ovarian cancer.

CRediT authorship contribution statement

SAB conceived and designed the study. PBP and AMM developed the monoclonal antibody. GSS, RSK, RRN, SSV, SCK, JKD and AMM performed experiments, interpreted results, executed statistical analyses, and contributed to manuscript writing. GSS, RSK and SAB organized the preliminary data and prepared the first manuscript draft and manuscript editing; the entire revised manuscript, figures and supplementary data were prepared by SSV, RSK, AMM and SAB. The work was supported by intramural grants to SAB.

The authors have declared no conflicts of interest

None of the authors report any conflict of interests. SAB, RSK, AMM and PBP have a patent granted – Indian Patent # 374,150: A MONOCLONAL ANTIBODY TARGETING THE TUMOR REGENERATIVE HIERARCHY.

Acknowledgments

All authors dedicate this manuscript to the memory of Dr. Parab who we lost recently to pancreatic cancer. The work was supported by intramural grants to SAB from NCCS, Pune and extramural grants from Department of Biotechnology, Government of India, New Delhi (BT/PR7186/MED/14/965/2006). Research fellowships were also availed as follows: RSK from Department of Biotechnology, New Delhi, India; GSS, SSV and SCK from Council of Scientific and Industrial Research, New Delhi, India; RRN from University Grants Commission, New Delhi India. We extend our gratitude to Prof. Judith Clements (Translational Research Institute, Australia) for providing the OVCA420, PEO14, OVCA432 and CAOV3 cell lines; Dr S. Mok (M. D. Anderson Cancer Center, TX) and Prof. Viktor Magdalen (Klinische Forschergruppe der Frauenklinik der TU München) for OV90 and OVMZ6 cell lines, and NCCS Repository for all the other cell lines used in the study. Technical assistance and support from the Proteomics, FACS, Imaging and Animal House facilities at NCCS are gratefully acknowledged.

Supplementary materials

Supplementary material associated with this article can be found, in the online version, at doi:10.1016/j.tranon.2021.101257.

References

[1] P.K. Raghav, Z. Mann, Cancer stem cells targets and combined therapies to prevent recurrence, Life Sci. 119465 (2021), https://doi.org/10.1016/j.lfs.2021.119465.
[2] J.E. Visvader, G.L. Lindeman, Cancer stem cells: current status and evolving complexities, Cell Stem Cell 10 (2012) 717–728, https://doi.org/10.1016/j.stem.2012.05.007.
[3] H.M. Zhou, J.G. Zhang, X. Zhang, Q. Li, Targeting cancer stem cells for reversing therapy resistance: mechanism, signaling, and prospective agents, Signal Transduct Target Ther 6 (2021) 62, https://doi.org/10.1038/s41392-020-00430-1.
[4] T. Shibue, R.A. Weinberg, EMT, CSCs, and drug resistance: the mechanistic link and clinical implications, Nat. Rev. Clin. Oncol. 14 (2017) 611–629, https://doi.org/10.1038/nrclinonc.2017.44.
[5] N. Vasan, J. Baselga, D.M. Hyman, A view on drug resistance in cancer, Nature 575 (2019) 299–309, https://doi.org/10.1038/s41586-019-1730-1.
[6] A. Ribas, J.D. Wolchok, Cancer immunotherapy using checkpoint blockade, Science 359 (2018) 1350–1355, https://doi.org/10.1126/science.aar4060.
[7] C.L. Ventola, Cancer Immunotherapy, Part 1: Current Strategies and Agents. P T 42 (2017) 375–383.
[8] X. Zhang, S. Liu, C. Guo, J. Zong, M.Z. Sun, The association of annexin A2 and cancers, Clin. Transl. Oncol. 14 (2012) 634–640, https://doi.org/10.1007/s12094-012-0855-6.
[9] A.R. Nazmi, G. Ozorowski, M. Pejic, J.P. Whitelegge, V. Gerke, H. Luecke, N-terminal acetylation of annexin A2 is required for S100A10 binding, Biol. Chem. 393 (2012) 1141–1150, https://doi.org/10.1515/hsz-2012-0179.
[10] S.S. Varankar, M. More, A. Abraham, et al., Functional balance between Tcf21-Slug defines cellular plasticity and migratory modalities in high grade serous ovarian cancer cell lines, Carcinogenesis 41 (2020) 515–526, https://doi.org/10.1093/carcin/bgz119.
[11] S.A. Bapat, A.M. Mali, C.B. Koppikar, N.K. Kurrey, Stem and progenitor-like cells contribute to the aggressive behavior of human epithelial ovarian cancer, Cancer Res. 65 (2005) 3025–3029, https://doi.org/10.1158/0008-5472.CAN-04-3931.
[12] R.R. Naik, A.K. Singh, A.M. Mali, M.F. Khirade, S.A. Bapat, A tumor deconstruction platform identifies definitive end points in the evaluation of drug responses, Oncogene 35 (2016) 727–737, https://doi.org/10.1038/onc.2015.130.
[13] R. Han, S. Gu, Y. Zhang, et al., Estrogen promotes progression of hormone-dependent breast cancer through CCL2-CCR2 axis by upregulation of Twist via PI3K/AKT/NF-kappaB signaling, Sci. Rep. 8 (2018) 9575, https://doi.org/10.1038/s41598-018-27810-6.
[14] Z. Wu, M.F. Gu, R.F. Zeng, Y. Su, S.M. Huang, Correlation between nasopharyngeal carcinoma tumor volume and the 2002 International Union Against Cancer tumor classification system, Radiat. Oncol. 8 (2013) 87, https://doi.org/10.1186/1748-717X-8-87.
[15] R.S. Kalra, S.A. Bapat, Expression proteomics predicts loss of RXR-gamma during progression of epithelial ovarian cancer, PLoS One 8 (2013) e70398, https://doi.org/10.1371/journal.pone.0070398.
[16] R.S. Kalra, S.A. Bapat, Proteomics to Predict Loss of RXR-gamma During Progression of Epithelial Ovarian Cancer, Methods Mol. Biol. (2019) 1–14, https://doi.org/10.1007/978-1-4939-9585-1_1, 2019.
[17] A.P. Kusumbe, S.A. Bapat, Cancer stem cells and aneuploid populations within developing tumors are the major determinants of tumor dormancy, Cancer Res. 69 (2009) 9245–9253, https://doi.org/10.1158/0008-5472.CAN-09-2802.
[18] R.S. Kalra, S.A. Bapat, Enhanced levels of double-strand DNA break repair proteins protect ovarian cancer cells against genotoxic stress-induced apoptosis, J Ovarian Res 6 (2013) 66, https://doi.org/10.1186/1757-2215-6-66.
[19] S.A. Bapat, A. Krishnan, A.D. Ghanate, A.P. Kusumbe, R.S. Kalra, Gene expression: protein interaction systems network modeling identifies transformation-associated molecules and pathways in ovarian cancer, Cancer Res. 70 (2010) 4809–4819, https://doi.org/10.1158/0008-5472.CAN-10-0447.
[20] S.C. Kamble, A. Sen, R.D. Dhake, A.N. Joshi, D. Midha, S.A. Bapat, Clinical Stratification of High-Grade Ovarian Serous Carcinoma Using a Panel of Six Biomarkers, J Clin Med 8 (2019), https://doi.org/10.3390/jcm8030330.
[21] S. Saha, G.P. Raghava, Prediction of continuous B-cell epitopes in an antigen using recurrent neural network, Proteins 65 (2006) 40–48, https://doi.org/10.1002/prot.21078.
[22] M.C. Jespersen, B. Peters, M. Nielsen, P. Marcatili, BepiPred-2.0: improving sequence-based B-cell epitope prediction using conformational epitopes, Nucleic. Acids. Res. 45 (2017) W24–W29, https://doi.org/10.1093/nar/gkx346.
[23] Y. El-Manzalawy, D. Dobbs, V. Honavar, Predicting flexible length linear B-cell epitopes, Comput Syst Bioinformatics Conf 7 (2008) 121–132.
[24] Ponomarenko J, H.H. Bui, W. Li, et al., ElliPro: a new structure-based tool for the prediction of antibody epitopes, BMC Bioinformatics 9 (2008) 514, https://doi.org/10.1186/1471-2105-9-514.
[25] S.A. Bapat, R.R. Naik, US Patent (2019), 20170067901. #.
[26] M.K. Myrvang, X. Guo, C. Li, L.V. Dekker, Protein interactions between surface annexin A2 and S100A10 mediate adhesion of breast cancer cells to microvascular endothelial cells, FEBS Lett. 587 (2013) 3210–3215, https://doi.org/10.1016/j.febslet.2013.08.012.
[27] T.M. Noye, N.A. Lokman, M.K. Oehler, C. Ricciardelli, S100A10 and Cancer Hallmarks: structure, Functions, and its Emerging Role in Ovarian Cancer, Int. J. Mol. Sci. 19 (2018), https://doi.org/10.3390/ijms19124122.
[28] I. Aukrust, L.A. Rosenberg, M.M. Ankerud, et al., Post-translational modifications of Annexin A2 are linked to its association with perinuclear nonpolysomal mRNP complexes, FEBS Open Bio 7 (2017) 160–173, https://doi.org/10.1002/2211-5463.12173.
[29] L. Zheng, K. Foley, L. Huang, et al., Tyrosine 23 phosphorylation-dependent cell-surface localization of annexin A2 is required for invasion and metastases of pancreatic cancer, PLoS One 6 (2011) e19390, https://doi.org/10.1371/journal.pone.0019390.
[30] D.I. Staquicini, R. Rangel, L. Guzman-Rojas, et al., Intracellular targeting of annexin A2 inhibits tumor cell adhesion, migration, and in vivo grafting, Sci. Rep. 7 (2017) 4243, https://doi.org/10.1038/s41598-017-03470-w.
[31] V.M. Kim, A.B. Blair, P. Lauer, et al., Anti-pancreatic tumor efficacy of a Listeria-based, Annexin A2-targeting immunotherapy in combination with anti-PD-1 antibodies, J. Immunother. Cancer 7 (2019) 132, https://doi.org/10.1186/s40425-019-0601-5.
[32] A.W. Woodham, J.R. Taylor, A.I. Jimenez, et al., Small molecule inhibitors of the annexin A2 heterotetramer prevent human papillomavirus type 16 infection, J. Antimicrob. Chemother. 70 (2015) 1686–1690, https://doi.org/10.1093/jac/dkv045.
[33] K. Kesavan, J. Ratliff, E.W. Johnson, et al., Annexin A2 is a molecular target for TM601, a peptide with tumor-targeting and anti-angiogenic effects, J. Biol. Chem. 285 (2010) 4366–4374, https://doi.org/10.1074/jbc.M109.066092.
[34] F. Pi, H. Zhang, H. Li, et al., RNA nanoparticles harboring annexin A2 aptamer can target ovarian cancer for tumor-specific doxorubicin delivery, Nanomedicine 13 (2017) 1183–1193, https://doi.org/10.1016/j.nano.2016.11.015.
[35] C.Y. Wang, C.L. Chen, Y.L. Tseng, et al., Annexin A2 silencing induces G2 arrest of non-small cell lung cancer cells through p53-dependent and -independent

mechanisms, J. Biol. Chem. 287 (2012) 32512–32524, https://doi.org/10.1074/jbc.M112.351957.
[36] X. Feng, H. Liu, Z. Zhang, Y. Gu, H. Qiu, Z. He, Annexin A2 contributes to cisplatin resistance by activation of JNK-p53 pathway in non-small cell lung cancer cells, J. Exp. Clin. Cancer Res. 36 (2017) 123, https://doi.org/10.1186/s13046-017-0594-1.
[37] H. Jung, J.S. Kim, W.K. Kim, et al., Intracellular annexin A2 regulates NF-kappaB signaling by binding to the p50 subunit: implications for gemcitabine resistance in pancreatic cancer, Cell Death. Dis. 6 (2015) e1606, https://doi.org/10.1038/cddis.2014.558.
[38] S.H. Tan, D. Young, Y. Chen, et al., Prognostic features of Annexin A2 expression in prostate cancer, Pathology 53 (2021) 205–213, https://doi.org/10.1016/j.pathol.2020.07.006.
[39] N.A. Lokman, C. E. Pyragius, A. Ruszkiewicz, M.K. Oehler, C. Ricciardelli, Annexin A2 and S100A10 are independent predictors of serous ovarian cancer outcome, Transl Res 171 (2016) 83–95, https://doi.org/10.1016/j.trsl.2016.02.002, e81-82.
[40] X.H. Xu, W. Pan, et al., Association of annexin A2 with cancer development (Review), Oncol. Rep. 33 (2015) 2121–2128, https://doi.org/10.3892/or.2015.3837.
[41] K. Odunsi, J. Matsuzaki, S.R. James, et al., Epigenetic potentiation of NY-ESO-1 vaccine therapy in human ovarian cancer, Cancer Immunol. Res. 2 (2014) 37–49, https://doi.org/10.1158/2326-6066.CIR-13-0126.
[42] R.R. Weng, H.H. Lu, C.T. Lin, et al., Epigenetic modulation of immune synaptic-cytoskeletal networks potentiates gammadelta T cell-mediated cytotoxicity in lung cancer, Nat. Commun. 12 (2021) 2163, https://doi.org/10.1038/s41467-021-22433-4.
[43] C. Kantara, M.R. O'Connell, G. Luthra, et al., Methods for detecting circulating cancer stem cells (CCSCs) as a novel approach for diagnosis of colon cancer relapse/metastasis, Lab. Invest. 95 (2015) 100–112, https://doi.org/10.1038/labinvest.2014.133.
[44] S. Li, K.A. Goncalves, B. Lyu, L. Yuan, G.F. Hu, Chemosensitization of prostate cancer stem cells in mice by angiogenin and plexin-B2 inhibitors, Commun Biol 3 (2020) 26, https://doi.org/10.1038/s42003-020-0750-6.